Molecular and Cellular Neuroscience 49 (2012) 322–332

Contents lists available at SciVerse ScienceDirect

Molecular and Cellular Neuroscience

journal homepage: www.elsevier.com/locate/ymcne

Sensorimotor function is modulated by the serotonin receptor 1d, a novel marker for gamma motor neurons

Anders Enjin [a,1], Katarina E. Leão [a,1], Sanja Mikulovic [a], Pierre Le Merre [a], Warren G. Tourtellotte [b], Klas Kullander [a,*]

[a] Department of Neuroscience, Uppsala University, Box 587, 751 23 Uppsala, Sweden
[b] Department of Pathology and Neurology, Northwestern University, Feinberg School of Medicine, 303 E. Chicago Ave., Chicago, IL 60611, USA

ARTICLE INFO

Article history:
Received 24 August 2011
Revised 19 December 2011
Accepted 4 January 2012
Available online 17 January 2012

Keywords:
5-ht1d
Serotonin
Gamma motor neurons
Muscle spindle
Fusimotor system
Spinal cord
Proprioception
Motor behavior

ABSTRACT

Gamma motor neurons (MNs), the efferent component of the fusimotor system, regulate muscle spindle sensitivity. Muscle spindle sensory feedback is required for proprioception that includes sensing the relative position of neighboring body parts and appropriately adjust the employed strength in a movement. The lack of a single and specific genetic marker has long hampered functional and developmental studies of gamma MNs. Here we show that the serotonin receptor 1d (*5-ht1d*) is specifically expressed by gamma MNs and proprioceptive sensory neurons. Using mice expressing GFP driven by the *5-ht1d* promotor, we performed whole-cell patch-clamp recordings of *5-ht1d::GFP*$^{+}$ and *5-ht1d::GFP*$^{-}$ motor neurons from young mice. Hierarchal clustering analysis revealed that gamma MNs have distinct electrophysiological properties intermediate to fast-like and slow-like alpha MNs. Moreover, mice lacking *5-ht1d* displayed lower monosynaptic reflex amplitudes suggesting a reduced response to sensory stimulation in motor neurons. Interestingly, adult *5-ht1d* knockout mice also displayed improved coordination skills on a beam-walking task, implying that reduced activation of MNs by Ia afferents during provoked movement tasks could reduce undesired exaggerated muscle output. In summary, we show that *5-ht1d* is a novel marker for gamma MNs and that the 5-ht1d receptor is important for the ability of proprioceptive circuits to receive and relay accurate sensory information in developing and mature spinal cord motor circuits.

Introduction

Muscle spindles are innervated by group Ia and group II proprioceptive sensory neurons and signal the magnitude and rate of muscle stretch to interneurons and motor neurons (MNs) of the spinal cord. This information is then used to modulate the step cycle, facilitate step transition and regulate the amplitude of muscle contraction (Rossignol et al., 2006) leading to smooth and automatic movements (Cole and Sedgwick, 1992; Tourtellotte and Milbrandt, 1998). To understand neuronal circuitry, it is vital to identify the participating neuronal sub-populations and to dissect the function of the neurons at the molecular level (Kullander, 2005).

Gamma MNs of the spinal cord regulate the sensitivity of muscle spindles by exclusively innervating intrafusal muscle fibers. Gamma MNs share many features with the contraction-generating alpha and beta MNs such as neurotransmitter phenotype, muscle projection and location within the spinal cord (Kanning et al., 2010), but lack the direct Ia input, recurrent collaterals, and C-bouton synaptic input that is characteristic for alpha MNs (Eccles et al., 1960; Lagerback, 1985). Further, gamma MNs are characterized by their smaller soma size and lesser dendritic branching compared to alpha MNs (Burke et al., 1977; Strick et al., 1976; Westbury, 1982). Gamma MNs are suitable for studying sensorimotor-related modulations of spinal circuits since they, in contrast to beta MNs that innervates both intra- and extrafusal muscle fibers, only innervate intrafusal muscle spindles.

The development of proprioceptive circuits relies on the correct regulation of muscle spindles by gamma MNs. Such studies of gamma MNs during early development have been cumbersome due to the lack of a single, specific genetic marker for gamma MNs. Although recent work has identified several useful molecular markers for gamma MNs, these still rely on the differential expression of more than one protein and on complementary profiles of expression in alpha MN (Friese et al., 2009; Shneider et al., 2009b). Recently, several novel genetic MN markers have been identified, including a marker specific for fast MNs (Enjin et al., 2010). This study did not identify any gamma MN marker, however, based on the aforementioned studies and the specialized features of gamma MNs, we hypothesized that genes selectively expressed in gamma MNs should exist.

Here we set out to identify a molecular marker that can readily distinguish gamma from alpha MNs already during early postnatal

* Corresponding author.
E-mail address: klas.kullander@neuro.uu.se (K. Kullander).
[1] These authors contributed equally to this work.

1044-7431/$ – see front matter © 2012 Elsevier Inc. All rights reserved.
doi:10.1016/j.mcn.2012.01.003

life independent of other criteria. We found that the serotonin receptor 1d (*5-ht1d*) meets the requirements for such a marker. To characterize gamma MN membrane properties, we performed whole-cell patch clamp recording from *5-ht1d::GFP*-expressing MNs. Using statistical methods for analysis we show gamma MNs to constitute a subtype of MNs with distinct membrane properties at early stages. To further study the role of the serotonin receptor 5-HT1D expression by gamma MNs, during development of spinal cord circuits, we used mice with a genetic inactivation of *5-ht1d*. We show that *5-ht1d* knockout mice have reduced amplitude of the electrically evoked monosynaptic reflex and altered motor coordination on a balancing test, suggesting that 5-*ht1d* has a role in the development of spinal motor circuits.

Results

Molecular identification of gamma MNs

To find presumptive genes particularly expressed by gamma MNs, we screened the GENSAT database (http://www.gensat.org) for BAC transgenic lines with expression in small cells in the motor columns of the spinal cord. One mouse line, where GFP is driven by the promoter of serotonin receptor 1d (*5-ht1d*; also known as *htr1d,* official NCBI annotation), showed GFP-expression specific to small cells in the motor columns and was chosen for further studies as a candidate marker for gamma MNs.

In situ hybridization of sections from P11 wild type mice confirmed that *5-ht1d* mRNA was expressed in the motor columns in the spinal cord (Fig. 1A). *5-ht1d*-expressing cells were seen at all levels of the spinal cord and the expression was scattered throughout the motor column suggesting the expression was not specific to certain motor pools. Apart from the expression in motor columns, few cells in the ventral and dorsal horn expressed *5-ht1d* (Fig. 1A). *In situ* sections from the brainstem of adult wild type mice showed *5-ht1d* to be expressed in cranial motor nuclei ambiguous, oculomotoris, trochlearis and abducens, while expression was not detected in nucleus facialis and nucleus hypoglossus (Fig. 1B).

To confirm that *5-ht1d* mRNA was expressed by MNs, we performed double *in situ* hybridizations using a probe against the vesicular acetylcholine transporter (*VAChT*; also known as Slc18a3) as a motor neuron marker. The *5-ht1d*$^+$ cells in lateral motor column all co-expressed *VAChT,* constituting 28% of all MNs at lumbar levels (Fig. 1C, $n=266$ cells). Measurement of the soma area of *5-ht1d*$^+$ and *5-ht1d*$^-$ MNs showed that *5-ht1d* was expressed by 95% of the smallest MNs (100–200 μm^2), in 44% of MNs with a soma area of 200–400 μm^2 and not in motor neurons larger than 400 μm^2 (Fig. 1C). Thus, *5-ht1d* is expressed by small MNs at all levels of the spinal cord as well as in most cranial motor nuclei.

In knockout mice for the zinc-finger transcription factor early growth response 3 gene (*Egr3*), muscle spindles degenerate postnatally and by P11 small presumptive gamma MNs are absent (Enjin et al., 2010; Shneider et al., 2009b; Tourtellotte et al., 2001). Results from *in situ* hybridization of sections from P11 *Egr3*$^{-/-}$ knockout mice demonstrated that the numbers of cells in the motor column expressing *5-ht1d* was greatly reduced compared to *Egr3*$^{+/+}$ mice (Fig. 1D) (wt: 11.19 ± 1.13, $n=21$; KO: 0.93 ± 0.29, $n=14$; $p<0.0001$). Taken together, the expression of *5-ht1d* in motor columns, in small motor neurons and the diminished expression in *Egr3*$^{-/-}$ motor columns suggested that *5-ht1d* is expressed by gamma MNs.

5-ht1d mRNA was also expressed in a subpopulation of sensory neurons in dorsal root ganglia (DRG). Potentially, *5-ht1d* could be expressed in the sensory part of the proprioceptive system as well. To determine if the *5-ht1d*-expressing cells were proprioceptive sensory neurons, we performed immunohistochemistry on sections from mice from the *5-ht1d::GFP* mouse line (at P2) and analyzed whether

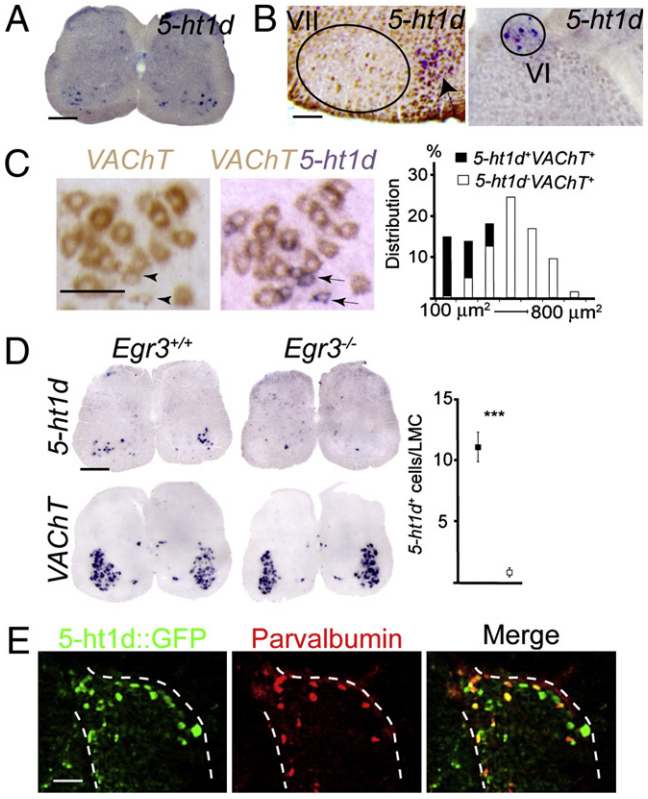

Fig. 1. *5-ht1d* marks gamma motor neurons and a subset of proprioceptive sensory neurons. (A) *In situ* hybridization on P11 lumbar spinal cord section showing expression of *5-ht1d* in the motor columns. (B) *In situ* hybridization of adult brain sections showing no detectable expression of *5-ht1d* in the facial nucleus (VII; left) while expression can be detected in a few cells in the abducens nucleus (VI; right). Arrow indicates expression in lateral paragigantonuclear nucleus. (C) Double *in situ* hybridization after development of *VAChT* alone (left) and after development of *5-ht1d* on the same section (middle) shows co-expression of *5-ht1d* and *VAChT* in a subset of motor neurons in P11 lumbar spinal cord. (right) Histogram of soma area estimation of *5-ht1d*$^+$*VAChT*$^+$ (black bars) and *5-ht1d-VAChT*$^+$ (white bars) neurons. (D) Expression of *5-ht1d* in P11 *Egr3*$^{+/+}$ (top left) and *Egr3*$^{-/-}$ (top middle) lumbar spinal cord. Expression of *VAChT* in P11 *Egr3*$^{+/+}$ (bottom left) and *Egr3*$^{-/-}$ (bottom middle) lumbar spinal cord. Quantification of *5-ht1d*-expressing cells in lumbar lateral motor column (LMC) shows a significant reduction in *Egr3*$^{-/-}$ mice (right; $p<0.0001$, Mann–Whitney *U*-test, mean ± SEM). (E) Expression of GFP (left), Parvalbumin (middle) and merged image (right) in lumbar dorsal root ganglia from P2 *5-ht1d::GFP* mice.

GFP labeled cells also expressed the proprioceptive marker Parvalbumin (Gong et al., 2003; Honda, 1995). The *5-ht1d::GFP* mouse showed expression of GFP in motor columns and in dorsal root ganglia (Fig. 1E) resembling the *5-ht1d* mRNA expression. *5-ht1d::GFP* co-stained with 78% of Parvalbumin$^+$ cells at thoracic, lumbar and sacral levels ($n=437$ Parvalbumin$^+$ cells from two mice). Thus, *5-ht1d* marks small MNs in the spinal cord as well as a large fraction of proprioceptive sensory neurons in dorsal root ganglia.

Electrophysiological character of 5-ht1d$^+$ *MNs*

Using whole-cell patch clamp recordings we measured passive and active membrane properties of *5-ht1d::GFP*$^+$ gamma MNs in transverse spinal cord slices (at P0–P6). Firing properties were examined in whole-cell current clamp configuration of MNs with stable resting membrane potential (average -60.00 ± 2.03 mV for GFP$^+$ MNs, $n=8$, and -54.55 ± 1.35 mV for GFP$^-$ MNs, $n=20$). The membrane potential was routinely held at −60 mV by injecting a bias current to overcome difference in resting membrane potential. GFP$^+$ cells that were filled with biocytin (Fig. 2A, see b1 and b2) showed a less complex dendritic arbor with fewer branches compared to

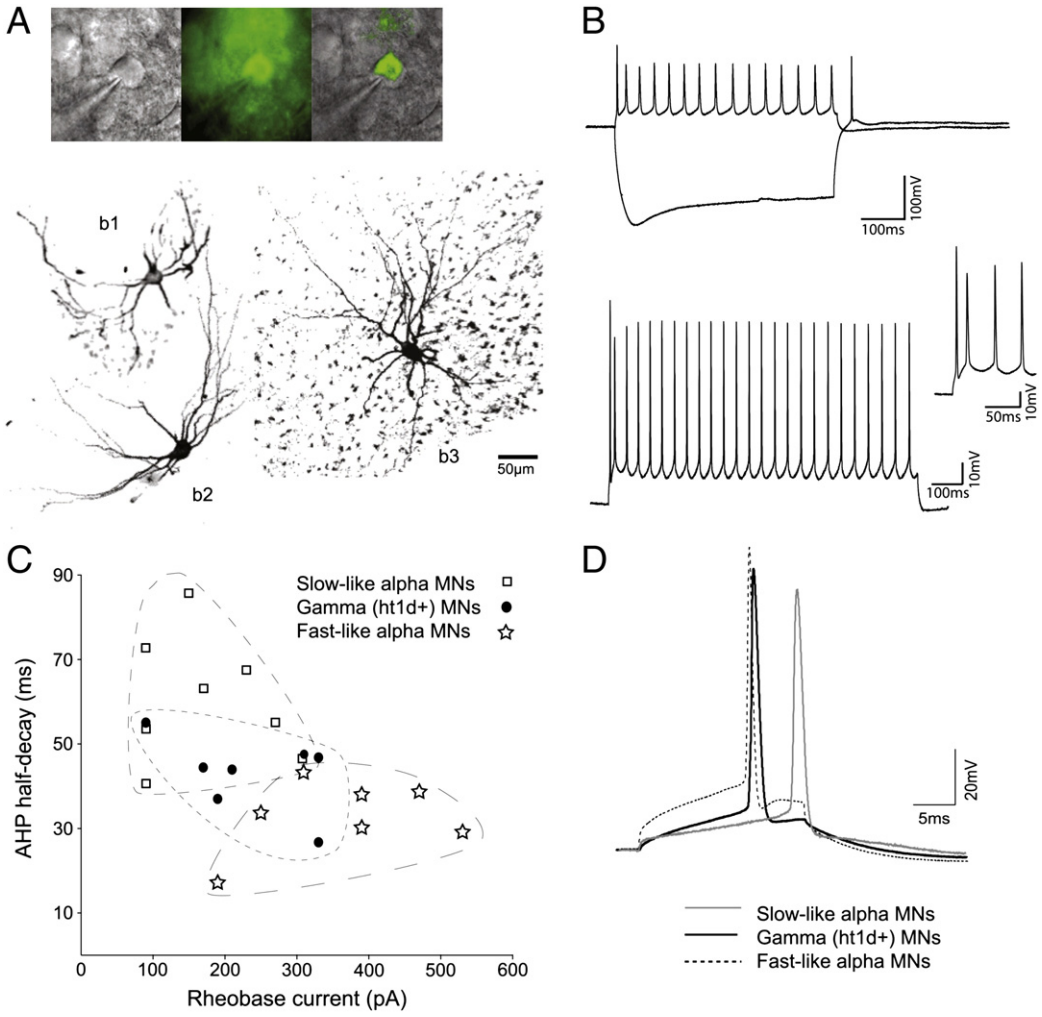

Fig. 2. Electrophysiological properties of *5-ht1d::GFP*$^+$ MNs. (A) top: Image of a patched *5-ht1d::GFP*$^+$ MN under bright-field light (left), fluorescence (middle) and merged (right). bottom: Cell in (A) filled with biocytin (b1) together with another *5-ht1d::GFP*$^+$ (b2) MN and a *5-ht1d::GFP*$^-$ (b3) MN. (B) top: Firing properties in response to a +50 pA current step showing regular spiking and to a −350 pA current step showing a depolarizing sag and rebound spike. Bottom: Firing in response to a +350 pA, 2 s duration, current step shows the initial doublet of spikes followed by regular spiking reaching a steady state frequency at the second half of the trace. inset: the initial doublet at higher magnification. (C) Scatterplot of rheobase current vs. after-hyperpolarization (AHP) half-decay time for gamma MNs (black circles), fast alpha MNs (stars) and slow alpha MNs (squares). (D) Example of action potentials from a gamma MN (black line), a fast-like alpha MN (dashed line) and a slow-like alpha MN (grey line) with representative rheobase value, AP half-width and delay to spike.

GFP$^-$ MNs (Fig. 2A, see b3). GFP$^+$ MNs displayed typical MN firing properties, with regular spiking in response to positive current injections, and a small hyperpolarizing sag, sometimes with a rebound spike upon termination, in response to a negative current step (Fig. 2B, top). In response to higher depolarizing current steps the initial doublet response becomes prominent, with the two first spikes in a train occurring with a very short interspike interval, as is typical for MNs (Fig. 2B, bottom). We further investigated if gamma MNs have distinct membrane properties, during the first postnatal week, that are distinguishable from other MNs. Beyond MNs being subdivided into alpha, beta and gamma MNs dependent on their innervation of muscle fibers, alpha MNs can be further subdivided into functional subgroups such as fast and slow type alpha MNs, based on the type of force generating muscle fiber they innervate (Kernell et al., 1999). We chose to compare gamma MNs to putative fast and slow alpha MNs as GFP$^-$ MNs recorded from most likely were alpha MNs (beta MNs being rare and small). Subgroups of alpha MNs have been shown to display different values for after hyperpolarization (AHP) and rheobase current, where AHP can be seen as the membrane hyperpolarization following an action potential and here a short AHP half-decay time is typical for fast type alpha MNs. Instead a longer duration AHP half-decay time is indicative of slow type alpha MNs. Rheobase current is the minimal square current pulse injection needed to reach the action potential threshold of a MN, and here fast-like alpha MNs usually require a large current to reach firing threshold, while a slow-like MN reach threshold potential in response to lower rheobase current. However, since MNs mature with age, with respect to electrophysiological properties, we could not predict subgroups of GFP$^-$ MNs based only on these two parameters. Instead, to compare gamma MNs properties to putative subclasses of alpha MNs we used 16 parameters (Supplementary Table 1), recorded in response to different current clamp protocols, to develop a clustering algorithm that could adequately group GFP$^-$ MNs with similar properties. Using agglomerative hierarchical clustering two clusters were found to give the optimal fit for the dataset (Supplementary Fig. 1). These two clusters corresponded well to previous published data of difference between fast and slow MNs (in respect to AHP half-decay time, rheobase current and input resistance) and GFP$^-$ MNs were therefore designated fast-like or slow-like MNs. There was no difference in mean postnatal age between these groups (*5-ht1d::GFP*$^+$ 2.38 ± 0.46, Fast-like 3.43 ± 0.69 and Slow-like 2.25 ± 0.77, $p = 0.4067$, one-way ANOVA, Supplementary Fig. 2). These groupings could be outlined in a scatterplot of AHP versus rheobase current for GFP$^+$ and GFP$^-$ MNs (Fig. 2C) where fast-like alpha MNs are similar

to chondrolectin-expressing fast MNs (Enjin et al., 2010). Here, gamma MNs show intermediate values for both AHP half-decay time and rheobase current in relation to fast-like or slow-like alpha MNs (Fig. 2C). Also for action potential properties gamma MNs were on average showing an intermediate action potential waveform (Fig. 2D). In detail, electrophysiological properties of *5-ht1d::GFP*$^{+}$ MNs were found to be significantly different from fast and slow alpha MN in respect to several properties: The mean input resistance for fast alpha MNs and slow alpha MNs were significantly different from gamma MNs ($p=0.00041$, one-way ANOVA). The initial doublet distance was different between gamma MNs and fast alpha MNs ($p=0.023$, Student's *t*-test). There was a difference in AP half-width of gamma MN and fast alpha MNs ($p=0.004$), and between fast and slow alpha MNs ($p=0.0004$). The AP delay was also significantly different between gamma MNs and fast alpha MNs ($p=0.049$) and between fast and slow alpha MNs ($p=0.0092$). Rheobase current was different between all three groups ($p=0.0049$, one-way ANOVA). After-hyperpolarization-time to peak was different between gamma MNs and slow alpha MNs ($p=0.011$, Student's *t*-test), as well as for slow alpha MNs and fast alpha MNs ($p=0.0022$, Student's *t*-test). Finally, the average AHP half-decay time, from AHP peak amplitude to the time when the potential had dropped half way to resting potential, was different between the three groups ($p=0.00043$, one-way ANOVA). The electrophysiological properties for gamma MNs, fast-like and slow-like alpha MNs are summarized in Table 1.

Molecular development of proprioceptive circuits in 5-ht1d$^{-/-}$ *mutant mice*

The contribution of the 5-HT1D receptor to the development of proprioceptive circuits was analyzed and compared between *5-ht1d*$^{-/-}$ knockout mice and littermate *5-ht1d*$^{+/+}$ controls. In *5-ht1d*$^{-/-}$ mice, the entire coding exon of *5-ht1d* is deleted and accordingly, spinal cords of adult *5-ht1d*$^{-/-}$ mice did not contain any cells expressing *5-ht1d* mRNA (Fig. 3A). Soma area measurements of *VAChT*$^{+}$ MNs in *5-ht1d*$^{-/-}$ spinal cords demonstrated that the size distribution of MNs were similar to *5-ht1d*$^{+/+}$ MNs, suggesting that gamma MNs are still present in the knockout mice (Fig. 3A-B).

The 5-HT1D receptor is suggested to be located presynaptically and serve as an autoreceptor on serotonergic neurons in the brain (Stamford et al., 2000). In addition, the 5-HT1D receptor has been implicated in functions related to axon guidance, presynaptic inhibition and peripheral anti-nociceptive response (Bonnin et al., 2007; Granados-Soto et al., 2010; Schwartz et al., 2005). Since the 5-HT1D receptor could be present on peripheral axons of gamma MNs and sensory neurons, we next investigated the expression of genes involved in serotonin synthesis in muscles. We found that mRNA for the serotonin-synthesizing enzymes tryptophan hydroxylase 1 (*Tph1*) and aromatic acid decarboxylase (*Aadc* also known as *Ddc*) as well as the vesicular monoamine transporter 2 (*VMAT2* also known as *Slc18a2*) was expressed in muscles of the hind limb in the P2 mouse (Fig. 4). The serotonin-related genes were found at the same location as the muscle spindle marker *Egr3*, when comparing the expression patterns in parallel sections. This suggests that muscle spindles may have the ability to synthesize and package serotonin in vesicles for release.

The 5-HT1D receptor is involved in the correct guidance of thalamocortical axons as they grow into the internal capsule (Bonnin et al., 2007). To evaluate if lack of 5-HT1D might have influenced the innervation of muscle spindles, we stained peripheral sensory afferent terminals using antibodies against vesicular glutamate transporter 1 (VGLUT1 also known as *Slc17a7*), muscular acetylcholine receptors with an antibody against bungarotoxin (BTX) and axons with β-tubulin III (TUJ1 also known as *Tubb3*). In *5-ht1d*$^{-/-}$ knockout mice, both proprioceptive and gamma motor-axons were present and innervated muscle spindles in similar patterns as to controls (Fig. 5A). Quantification of the number of *VAChT*$^{+}$ puncta in apposition to BTX^{+} postsynaptic terminals at muscle spindles stained with Calbindin (Hietanen-Peltola et al., 1992) did not reveal a difference between *5-ht1d*$^{-/-}$ knockout mice and littermate controls (Fig. 5B). Thus, we did not find evidence that the 5-HT1D receptor is required for muscle spindle innervation.

5-ht1d$^{-/-}$ *knockout mice show reduced electrically evoked monosynaptic reflex response in motor neurons*

Next, we wanted to see if *5-ht1d* is important for the central connectivity of proprioceptive circuits. The synapses of Ia afferents on MNs are distinguished by perisomatic expression of VGLUT1 (Betley et al., 2009) and as gamma MNs do not receive monosynaptic Ia input, they are not innervated by VGLUT1 containing synapses (Friese et al., 2009). Immunohistochemistry on spinal cord sections from adult (P30) *5-ht1d*$^{+/+}$ and *5-ht1d*$^{-/-}$ mice demonstrated similar amounts of VGLUT1 puncta on MN cell soma and proximal dendrites (wt: 5.30 ± 0.62, $n=57$; KO: 6.10 ± 0.68, $n=51$; $p=0.33$) (Fig. 6A) suggesting that alpha MN (and beta MNs) receive normal contacts of Ia afferents even though 5-ht1d is knocked out. Moreover, the percentage of MNs that either lacked or had VGLUT1^{+} synapses on the cell body and proximal dendrites were similar between 5-HT1D null mutant mice and controls (chi-squared, $p=0.17$) (Fig. 6B), indicating similar distribution of gamma MNs and alpha MNs in control and knockout animals.

To assess any physiological implications of lacking 5HT1D receptors, we simulated the electrically evoked monosynaptic reflex response by stimulating the dorsal roots and recorded responses from the ventral roots in an *in vitro* spinal cord preparation (Fig. 6C). In spinal cords from *5-ht1d*$^{-/-}$ mice (P2-P6), we observed a characteristic pattern of the monosynaptic ventral root response with a peak response corresponding primarily to Ia afferent synapses on MNs, and a second wider peak with longer latency corresponding to polysynaptic activation of MNs (Fig. 6D). Quantification of the monosynaptic peak (see methods) revealed significantly smaller amplitude in *5-*

Table 1
Membrane properties of gamma MNs (5-ht1d::GFP+, $n=8$), fast alpha MNs ($n=7$) and slow alpha MNs ($n=8$).

Property	Gamma	Fast-like	Slow-like	*P* value
Input resistance (MΩ)	82.60 ± 12.66	56.75 ± 5.36	132.83 ± 13.59	$<0.001^{*}$
Initial doublet (ms)	24.31 ± 5.13	43.38 ± 7.17	28.96 ± 6.08	$<0.05^{a}$
Firing frequency (Hz)	22.50 ± 1.58	22.02 ± 2.22	25.27 ± 2.73	NS
AP threshold (mV)	-37.03 ± 2.02	-33.33 ± 3.99	-34.88 ± 2.35	NS
AP half-width (ms)	0.72 ± 0.04	0.57 ± 0.02	0.82 ± 0.05	$<0.01^{a}$, $<0.001^{b}$
AP delay (ms)	19.87 ± 1.33	15.43 ± 2.21	22.43 ± 1.49	$<0.05^{a}$, $<0.01^{b}$
Rheobase current (pA)	235.00 ± 30	361.43 ± 45.33	175.00 ± 30.65	$<0.01^{*}$
AHP amplitude (mV)	3.49 ± 0.63	3.93 ± 0.49	4.16 ± 0.68	NS
AHP time to peak (ms)	19.97 ± 1.77	17.24 ± 1.32	30.24 ± 3.32	$<0.05^{a}$, $<0.01^{b}$
AHP half-decay time (ms)	43.01 ± 3.38	32.90 ± 3.22	60.61 ± 5.17	$<0.001^{*}$

* Indicates significant difference between all (one-way ANOVA); a indicates significant difference between Gamma and Fast (Student's *t*-test); b indicates significant difference between Fast and Slow (Student's *t*-test); NS, not significant. Values show ± standard error of the mean (S.E.M).

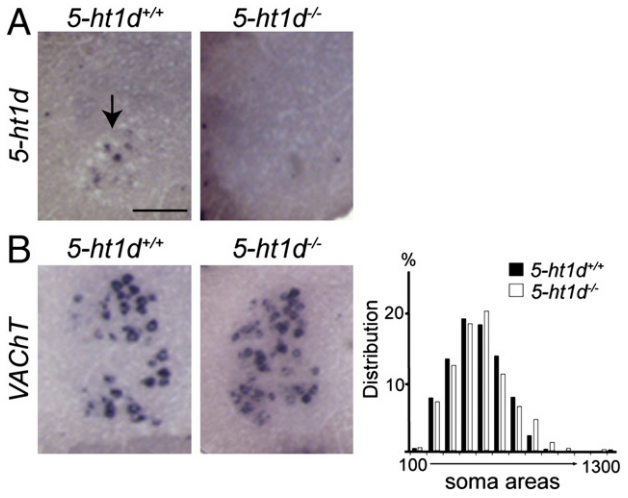

Fig. 3. *5-ht1d* is not required for gamma motor neuron survival. (A) *In situ* hybridization on adult lumbar spinal cord section showed expression of *5-ht1d* mRNA in *5-ht1d*$^{+/+}$ lateral motor columns. No cells positive for *5-ht1d* mRNA were found in *5-ht1d*$^{-/-}$ spinal cords. (B) *In situ* hybridization on adult lumbar spinal cord section of *VAChT* mRNA present in *5-ht1d*$^{+/+}$ and *5-ht1d*$^{-/-}$ lateral motor columns (left). Histogram showing frequency distribution of *VAChT*$^{+}$ motor neuron soma areas in the lateral motor column from adult *5-ht1d*$^{+/+}$ and *5-ht1d*$^{-/-}$ spinal cord sections (right).

ht1d$^{-/-}$ mice compared to control mice (Fig. 6E, $p=0.034$), while no difference in the latency was found (Fig. 6E). In contrast, the polysynaptic peak was equal between groups comparing the latency, amplitude and curve area (Fig. 6F). Thus, our data suggest that the 5HT1D receptor is involved in the proper development of the monosynaptic features of sensory-evoked activation of motor neurons.

5-ht1d$^{-/-}$ *mice have improved motor coordination*

To examine if the abnormal development of proprioceptive circuits would affect the motor behavior of *5-ht1d*$^{-/-}$ knockout mice, we investigated different aspects of motor coordination. There was no difference in weight between knockouts and control animals (*5-ht1d*$^{+/+}$: 30.6 ± 1.57 g., *5-ht1d*$^{-/-}$: 32.08 ± 1.95 g., $n=10$ animals per genotype, $p=0.55$) that could otherwise bias the test results. In a Rotarod test, a test for coordination and balance, no difference in performance was observed between *5-ht1d*$^{-/-}$ mice and control littermates (Fig. 7A). In contrast, when the mice were challenged in a beam walking balancing task, which require a higher precision in foot placement, the *5-ht1d*$^{-/-}$ knockout mice outperformed control littermates (number of slips per trials in *5-ht1d*$^{+/+}$: 1.0 ± 0.30, $n=8$; and *5-ht1d*$^{-/-}$: 0.24 ± 0.16, $n=7$; $p=0.040$) (Fig. 7B). There was no difference in time to cross the beam between *5-ht1d*$^{-/-}$ knockout mice and control mice (Fig. 7B). In addition, in a hanging wire challenge, testing for motor strength and coordination, 7 out of 10 *5-ht1d*$^{-/-}$ knockout mice climb onto the wire in less than 1 second compared to control littermates where 2 out of 9 climbed the wire in less than one second ($p=0.037$) (Fig. 7C). Thus, the *5-ht1d*$^{-/-}$ knockout mouse displays improved motor coordination in response to certain motor challenges.

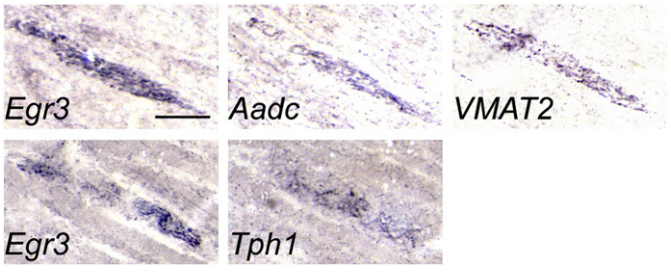

Fig. 4. Serotonin-related genes are expressed by muscle spindles. Images of *in situ* hybridization experiments of the same anatomical location in serial sections of P2 hind limb muscle tissue stained for the muscle spindle marker *Egr3* and the serotonin-related genes *Aadc* and *VMAT2* (top row) and *Tph1* (bottom row).

Discussion

5-ht1d-expression in gamma motor neurons

Several characteristics suggest that *5-ht1d* mRNA is expressed by gamma MNs. First, *5-ht1d* was only expressed in the smallest MNs. In cats and mice, gamma MNs are the smallest MNs (Bryan et al., 1972; Burke et al., 1977; Friese et al., 2009; Shneider et al., 2009b). Second, we found that *5-ht1d* mRNA was expressed by 28% of the total number of MNs at all levels of the spinal cord and in all somatic motor columns, in agreement with previous studies estimating the relative gamma MN population size to 25–30% (Burke et al., 1977; Friese et al., 2009; Shneider et al., 2009b). Third, in *Egr3*$^{-/-}$ mutants, where gamma MNs degenerate after birth (Enjin et al., 2010; Tourtellotte and Milbrandt, 1998; Tourtellotte et al., 2001), cells in the motor columns expressing *5-ht1d* mRNA were almost completely absent. Fourth, in the brainstem, *5-ht1d* was expressed in cranial motor nuclei known to innervate eye muscles that contain many muscle spindles, such as oculomotoris and abducens, while it was not expressed in the facial motor nucleus, which innervates muscles of facial expression reported to lack muscle spindles (Whitehead et al., 2005).

It remains to determine whether *5-ht1d* may also be expressed by beta MNs. However, in *Egr3*$^{-/-}$ knockout mice, where gamma MNs degenerate, beta MNs survive (Shneider et al., 2009b). In such mutants, we found that *5-ht1d*-expression was reduced to less than one cell per lateral motor column. Although a precise estimation of the proportion of beta MNs in the spinal cord remains elusive, observations in the adult cat suggests beta MNs to innervate 40–70% of muscle spindles, presumably constituting more than 1 cell per lateral motor column in a 60 μm section (Emonet-Denand et al., 1975; Scott et al., 1995). Therefore, we find it unlikely that *5-ht1d* mRNA is expressed by beta MNs.

Membrane properties of gamma motor neurons

With a single molecular marker for gamma MNs expressed early in development, it is possible to target gamma MNs in neonatal mouse tissue slices without the need for post hoc staining to confirm MN type (Friese et al., 2009; Shneider et al., 2009a,b). Using *5-ht1d::GFP*$^{+}$ mice we measured resting membrane properties and firing properties of gamma MNs. In contrast to the vast literature on the electrophysiological character of alpha MNs, similar studies of gamma MNs have been limited (Burke et al., 1994). It is known that gamma MNs have a smaller soma area, different dendrite morphology and slower conduction velocity compared to alpha MNs (Kanning et al., 2010; Shneider et al., 2009b; Westbury, 1982). Here, using the 5-ht1d marker we investigated if any differences in basic electrophysiological properties of gamma MNs and alpha MNs, with alpha MNs divided into the functional subgroups of fast and slow (Gardiner, 1993; Zengel et al., 1985) could be discerned in MNs from young mice. We chose to compared gamma MNs to the fast and slow subtype of alpha MN (Kernell et al., 1999) since an average value of neurons from different subgroups of alpha MNs could obscure our data, due to the small sample of MNs in this study. It is known that slow MNs respond to a lower rheobase current, have a larger AHP half-decay time and a higher input resistance than fast MNs (Zengel et al., 1985; Gardiner, 1993; Comery et al., 2000; Enjin et al., 2010), but an absolute cut-off limit between fast and slow motor neurons with respect to these properties has not been defined. Early in development, a single parameter may also not suffice to divide MN into

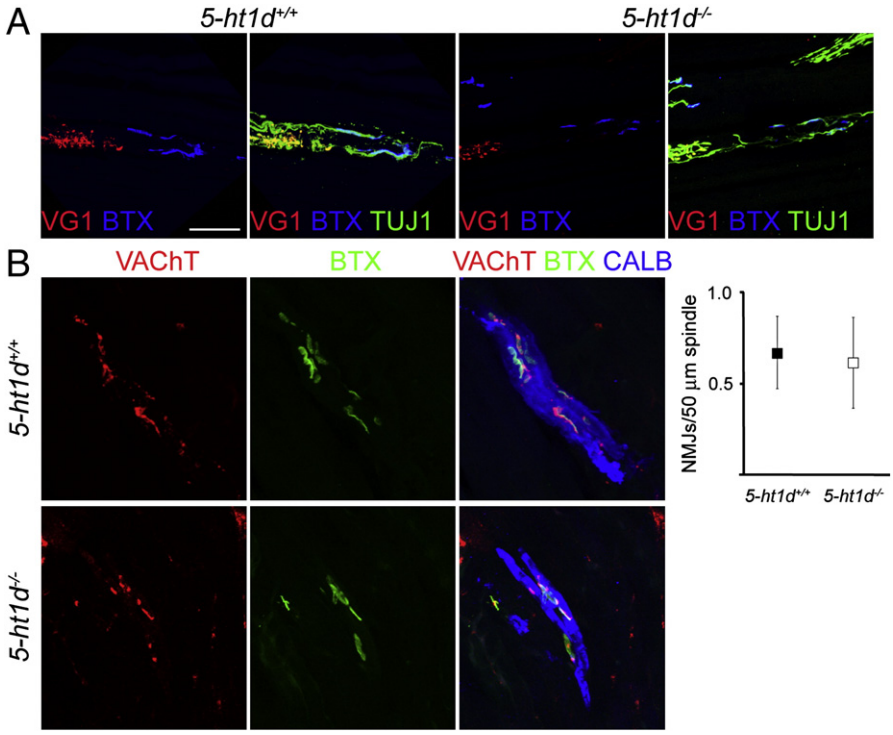

Fig. 5. Normal innervation of muscle spindles in *5-ht1d*$^{-/-}$ mice. (A) Confocal images of muscle spindles in the tibialis anterior muscle from P13 *5-ht1d*$^{+/+}$ (left) and *5-ht1d*$^{-/-}$ (right) mice. Sensory axons (VGLUT1^{+}TUJ1^{+}) and gamma motor axons (VGLUT1^{-}TUJ1^{+}) were present and distributed similarly in the muscle spindles of control and *5-ht1d*$^{-/-}$ mice . Bungarotoxin (BTX) binds to postsynaptic receptors of motor synapses. (B) Confocal images of motor neuron synapses in muscle spindles visualized with Calbindin (muscle spindle fiber), *VAChT* (presynaptic motor terminal) and BTX (postsynaptic motor terminal). Quantification of *VAChT*$^{+}$ BTX^{+} neuromuscular junctions on muscle spindles showed a similar motor innervation between *5-ht1d*$^{-/-}$ mice and control mice (mean ± SEM, two-tailed Student's *t*-test, $p = 0.86$).

subpopulations. To circumvent this, we used hierarchal clustering analysis to group neurons using both passive and active electrophysiological parameters. We did not try to correlate chondrolectin expression with alpha MN subtype (Enjin et al., 2010), as this was not the aim of this study, although we see that it could have been fit to use as a further validation of MN sub-classification.

GFP^{+} gamma MN membrane properties were found intermediate to the fast and the slow alpha MN properties of this study, and significantly different from both alpha MN types with respect to input resistance, rheobase current and AHP half-decay time. Input resistance is determined by cell size, but also by the expression of leak channels or voltage-gated ion channels active at resting membrane potential, such as the hyperpolarization-activated cation current (I_h) (Pape, 1996). The rheobase current is set by the amount of depolarization needed for reaching the voltage threshold, the input resistance and slow non-linear properties of the membrane, such as voltage-gated channels active at sub-threshold potential. The AHP is largely shaped by a Ca^{2+}-dependent K^{+} current, which contribute to setting the appropriate firing frequency of an alpha motor neuron, related to the contractile frequency of the muscle it innervates (Gardiner, 1993; Kanning et al., 2010). Despite the differences seen in these properties, we did not see a difference in firing frequency between GFP^{+} and GFP^{-} MNs in response to long current injections. This is not surprising since the firing probability (and hence firing frequency) of an individual neuron is determined by several factors including its AHP, input resistance and rheobase current. Therefore, the sum of these parameters in gamma MNs may still generate a similar firing pattern to alpha MNs in young mice. The similarity in firing properties of gamma and alpha MNs thus emphasizes the need for a specific gamma MN marker.

MN electrophysiological parameters are more homogeneous during early postnatal stages and diversify as development proceeds (Nakanishi and Whelan, 2010). Nevertheless, based on the data presented here, we propose that MNs can be divided into gamma, fast alpha and slow alpha MNs already in early postnatal mice based on both molecular and electrophysiological profile. The specific gene expression of *5-ht1d* at this stage suggests that there are genetic programs active relatively early in development that may participate in shaping different MN characteristics. Our previous study suggest that fast MNs can be distinguished from slow MNs based on electrophysiological properties and expression of chondrolectin at early postnatal stages, and that ERRβ may constitute a marker for slow MNs (Enjin et al., 2010). This may consequently lead to the development of an electrophysiological and gene expression code of MN subtypes during the early postnatal period.

The role of 5-ht1d in development and function of spinal motor circuits

We further hypothesized that 5-HT1D may be important for the development of spinal cord motor circuits, since serotonin has, apart from its classical role as a neuromodulator, many implications for the development of the nervous system. Disturbed serotonin signaling affects cell survival (Stankovski et al., 2007), axon guidance (Bonnin et al., 2007; Haydon et al., 1984) and development of neural circuits in the spinal cord and cerebral cortex (Gaspar et al., 2003; Pflieger et al., 2002). Furthermore, muscle-derived signals are important for proper tuning of synaptic strength between Ia afferents and MNs (Frank and Wenner, 1993; Mentis et al., 2010). We found expression of the serotonin related genes *Tph1*, *Aadc* and *VMAT2* in muscle spindles of young mice, which may indicate that developing sensorimotor synapses are modulated by serotonin, and that this modulation may be disrupted in *5-ht1d*$^{-/-}$ mutants. However, in *5-ht1d*$^{-/-}$ knockout animals, we did not observe any loss of gamma MNs nor any loss of motor and sensory innervation onto muscle spindles. If this is due to compensatory factors during development or whether 5-HT1D is dispensable for cell survival and muscle spindle innervation remains to be clarified.

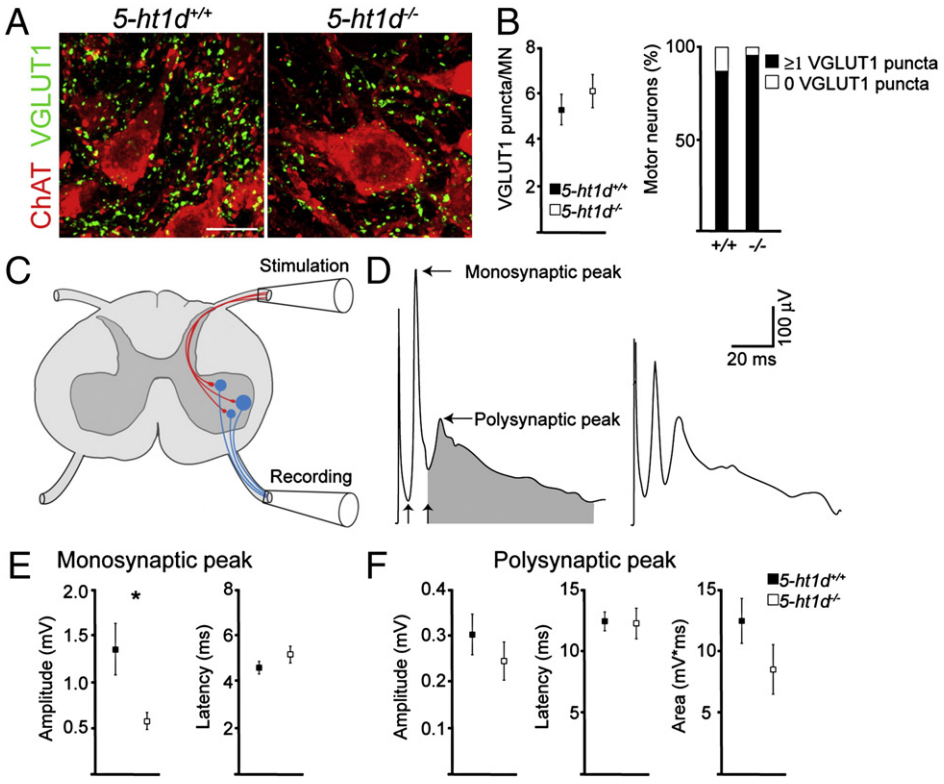

Fig. 6. *5-ht1d*$^{-/-}$ mice show reduced amplitude of monosynaptic sensorimotor connections. (A) VGLUT1^{+} contacts on ChAT^{+} motor neurons in adult (P30) thoracic spinal cord of *5-ht1d*$^{+/+}$ and *5-ht1d*$^{-/-}$ mice (left). (B) Quantification of VGLUT1^{+} contacts on motor neurons (left; *5-ht1d*$^{+/+}$, $n=57$, and *5-ht1d*$^{-/-}$, $n=51$, from 3 animals per genotype; Mann–Whitney *U*-test, $p=0.33$). Bar graph illustrating the ratio of motor neurons with (black) and without (white) detectable VGLUT1 contacts (right, *5-ht1d*$^{+/+}$, $n=57$, and *5-ht1d*$^{-/-}$, $n=51$, from 3 animals per genotype; Chi-squared test, $p=0.17$). (C) Schematic of experimental setup for recording responses in ventral root after dorsal root stimulations. (D) Example of averaged responses in L3 ventral roots from a P5 *5-ht1d*$^{+/+}$ (left) and a P3 *5-ht1d*$^{-/-}$ (right) mouse. Horizontal arrows indicate monosynaptic and polysynaptic peaks, vertical arrows indicate onset of monosynaptic and polysynaptic episodes. Shaded area indicates part of plot used to estimate polysynaptic area. (E) Graph of amplitude (left) and latency (right) of monosynaptic peak in *5-ht1d*$^{+/+}$ mice and *5-ht1d*$^{-/-}$ mice (Mean ± SEM, Students *t*-test, $p=0.034$ (amplitude), $p=0.17$ (latency), $n=10$ *5-ht1d*$^{+/+}$ mice and $n=7$ *5-ht1d*$^{-/-}$ mice). (F) Graph of amplitude (left), latency (middle) and area (right) of polysynaptic peak in neonatal *5-ht1d*$^{+/+}$ mice and *5-ht1d*$^{-/-}$ mice (Mean ± SEM, Students *t*-test, $p=0.35$ (amplitude), $p=0.88$ (latency), $p=0.16$ (area) $n=10$ *5-ht1d*$^{+/+}$mice and $n=7$ *5-ht1d*$^{-/-}$ *mice).*

We did observe a functional effect on sensorimotor connections in the *5-ht1d*$^{-/-}$ mouse. The amplitude of the monosynaptic response to dorsal root stimulation in MNs is reduced by approximately 50% in *5-ht1d*$^{-/-}$ mutants. We found Ia-derived VGLUT1-expression on presumable alpha MNs to be normal in *5-ht1d*$^{-/-}$ mutants, although VGLUT1-expression was only assessed on soma and proximal dendrites. Whether *5-ht1d*$^{-/-}$ mice have altered VGLUT1-expression on distal dendrites, due to developmental regulatory processes was not assessed here. Therefore, the reduced amplitude of the electrically evoked monosynaptic reflex may be due to such altered synaptic pruning on distal dendrites, or, reflect a role for 5-HT1D receptor signaling in setting the magnitude of monosynaptic proprioceptive activation of MNs. In accordance with a role for 5-HT1D, intramuscular injection of serotonin in hind limb muscles of the adult cat has demonstrated an increased excitability of gamma MNs, suggesting that serotonin receptors in muscles can influence the activity in proprioceptive circuits (Djupsjobacka et al., 1995; Jovanovic et al., 1990).

A reduced electrically evoked monosynaptic reflex has been seen in other mutant mice (Chen et al., 2002; Shneider et al., 2009a), which display an ataxic gait and abnormal posture. In stark contrast, we find an improved motor coordination in *5-ht1d* mutants. The muscle spindle morphology, innervation and VGLUT1 synapse count on MNs was normal in *5-ht1d*$^{-/-}$ mutants, whereas *Egr3, Nt-3* and *Erbb2* mouse mutants, in addition to the impaired electrically evoked

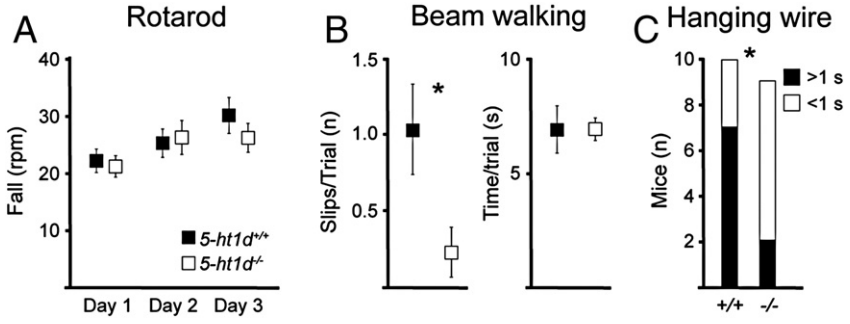

Fig. 7. Improved motor coordination in *5-ht1d*$^{-/-}$ mice. (A) Graph of the max rotational speed on the rotarod before fall for adult *5-ht1d*$^{+/+}$ mice and *5-ht1d*$^{-/-}$ mice (Mean ± SEM, 2-way ANOVA, $p=0.58$, $n=10$ *5-ht1d*$^{+/+}$mice and $n=10$ *5-ht1d*$^{-/-}$ mice). (B) Hind limb slips when running over a 12 mm beam (left) and time spent crossing the beam (right) of *5-ht1d*$^{+/+}$ mice and *5-ht1d*$^{-/-}$ mice (Mean ± SEM, Students *t*-test, $p=0.040$ (slips), $p=0.99$ (time) $n=8$ *5-ht1d*$^{+/+}$mice and $n=7$ *5-ht1d*$^{-/-}$ mice). (C) Time spent climbing onto a horizontal hanging steel wire with the hind paws in *5-ht1d*$^{+/+}$ (black) and *5-ht1d*$^{-/-}$ (white) mice (Chi-square test, $p=0.037$, $n=10$ *5-ht1d*$^{+/+}$ mice and $n=9$ *5-ht1d*$^{-/-}$ mice).

monosynaptic reflex, display abnormal muscle spindle development and have a reduced number of VGLUT1 synapses on motor neurons (Chen et al., 2002; Shneider et al., 2009a; Tourtellotte and Milbrandt, 1998). It is likely that the ataxic gait comes from a deficiency in peripheral activation of sensory neurons or diminished number of VGLUT1 synapses rather than in a reduced synaptic strength at the Ia afferent-MN synapse. More so, we show here that a reduction of the electrically evoked monosynaptic reflex amplitude alone does not seem to severely impair motor control.

What role does the amplitude of the H-reflex response have in skilled locomotion? In humans, the amplitude of the H-reflex is modulated during different gaits and is smaller during beam walking than when walking on a treadmill (Edamura et al., 1991; Llewellyn et al., 1990). In cats, the EPSP generated in MNs by Ia afferents is presynaptically inhibited during locomotion (Gosgnach et al., 2000). A reduced activation of MNs by Ia afferents during difficult movement tasks could thereby reduce hyper-excitation of MNs in order to prevent undesired exaggerated muscle output. Thus, the smaller amplitude of the electrically evoked monosynaptic reflex observed in the *5-ht1d*$^{-/-}$ mutant mice may therefore further "prime" skilled walking, by reducing the excitability of proprioceptive circuits, tentatively explaining the enhanced motor coordination seen in these mice.

In conclusion, we identified the serotonin receptor 1d (*5-ht1d*) as a novel molecular marker of gamma MNs in mouse spinal cord. Using *5-ht1d::GFP*$^{+}$ mice we recorded electrophysiological properties of gamma MNs during the first postnatal week and found them to be intermediate to fast-like and slow-like alpha MN characteristics. In addition, using a genetic inactivation of the *5-ht1d* receptor we observed a deficient development of the monosynaptic (H-) reflex and enhanced motor coordination of adult mice when performing a beam-walking test suggesting that 5-HT1D is involved in development and function of spinal motor circuits.

Experimental methods

Mice

5-ht1d$^{+/-}$ and *5-ht1d::GFP* mice were obtained from the Mutant Mouse Regional Resource Center (MMRRC) and genotyped using PCR with the following primers: wt CTGCCAAACCAGTCCCTAGAAG and GCAGCACGATGTCAGAAGAC; mutant GCAGCG CATCGCCTTCTATC and AACCCGGGTCTCAGAGAAATGGCA; GFP CCTACGGCGTGCAGTGCTTCAGC and CGGCGAGCTGCACGCTGCGTCCTC. *Egr3*$^{-/-}$ mice have been described previously (Tourtellotte and Milbrandt, 1998). Wild type tissue for *in situ* hybridization in Figs. 1 and 4 was taken from C57/Bl6 mice. All animal procedures were approved by the appropriate local Swedish ethical committee (permit C79/9) and The Northwestern University Institutional Animal Care and Use Committee, USA.

In situ hybridization and immunofluorescence

In situ hybridization and immunohistochemistry were performed as previously described (Enjin et al., 2010). The following probes were used: *5-ht1d* (GeneBank accession number NM_008309.4, nucleotides 1652–2842), Vesicular acetylcholine transporter (*VAChT*) (Wallen-Mackenzie et al., 2006), zinc-finger transcription factor early growth response 3 (*Egr3*) (GeneBank accession number NM_018781.2, nucleotides 219–1084), tryptophan hydroxylase 1 (*Tph1*) (Probe recognizes both isoforms; GeneBank accession number NM_009414.2, nucleotides 1229–2027 and GeneBank accession number NM_001136084.1, nucleotides 889–1732), aromatic acid decarboxylase (*Aadc*) (GeneBank accession number NM_016672, nucleotides 608–1615) and Vesicular monoamine transporter 2 (*VMAT2*) (Hermanson et al., 2003). The following antibodies were used; polyclonal goat anti-Choline Acetyltransferase (ChAT) (1:100; AB144P, Milipore), polyclonal goat anti-*VAChT* (1:500, AB1578, Milipore), polyclonal rabbit anti-Vesicular glutamate transporter 1 (VGLUT1) (1:500, 135002, Synaptic Systems), polyclonal rabbit- and guinea pig anti-VGLUT1 (1:300 both, (Fujiyama et al., 2001)), polyclonal rabbit anti-Calbindin (1:5000, CB38, Swant), monoclonal mouse anti-Parvalbumin (1:500, MAB1572, Chemicon), monoclonal rabbit anti-β-tubulin III (TUJ1) (1:1000, TUJ1-1-15-79, Covance) and Alexa 488-conjugated bungarotoxin (1:1000, B13422, Invitrogen). Prior to staining with the Parvalbumin antibody, tissue was treated with AffiniPure Fab Fragment Goat Anti-Mouse IgG ($H^{+}L$) (1:10, 115-007-003, Jackson immunoresearch) over night at 4 °C to block endogenous mouse IgG's.

Electrophysiology

5-ht1d::GFP mice (P0–P6) were anesthetized by hypothermia (<P3) or with Isoflurane (2-chloro-2-(difluoromethoxy)-1,1,1-trifluoroethane) (>P3), rapidly decapitated and the spinal cord was dissected in ice-cold solution that mimic the intracellular medium (Dugue et al., 2005) containing the following (in mM): 130K-Gluconate, 15 KCl, 0.05 EGTA, 20 HEPES, 25 Glucose, with pH adjusted to 7.2 by NaOH. The free-floating spinal cord was rapidly transferred to a precooled slicing chamber and stabilized in an upright position onto an agar block using 20% gelatin, and the chamber was filled with ice-cold dissection solution. Transverse slices (270–300 μm) of the lumbar region of the spinal cord were made using a vibrating blade microtome (VT1000 S, Leica microsystems). Slices were collected and incubated for 45 min–1 h in artificial cerebrospinal fluid (aCSF) (in mM: 128 NaCl; 4 KCl; 0.5 NaH_2PO_4; 21 $NaHCO_3$; 30 D-glucose; 1.5 $CaCl_2$; 1 $MgSO_4$; equilibrated with 95% O_2, 5% CO_2) at 35 °C and subsequently held at room temperature (22–24 °C) for electrophysiological recordings. The spinal cord slices were placed into the recording chamber and superfused with oxygenated aCSF at a rate of 2–4 ml/min. Patch pipettes (3–5 MΩ) were pulled from borosilicate glass (GC15OF-10, Harvard apparatus) on a P97 Flaming/Brown puller (Sutter instruments, Novato, CA). The internal pipette solution contained (in mM: 130K-Gluconate; 7 NaCl; 0.1 EGTA; 10 HEPES; 0.3 $MgCl_2$; 2 ATP; 0.5 GTP) and the pH was adjusted to 7.2 using KOH. The liquid junction potential was not corrected for. MNs were visualized on a BX51WI Olympus microscope fitted with infrared differential interference contrast (DIC) optics and a Lambda LS Xenon Arc lamp (Sutter instruments) for fluorescent light. MNs were identified as *5-ht1d::GFP*$^{+}$ when cell soma contained green fluorescent protein (GFP). Alpha MNs were identified on their morphology and being GFP negative and with soma diameter larger than 25 μm. Exposure to fluorescent light was minimized due to potential photo-damage, and images were only collected after electrophysiological properties had been recorded. DNA from tail tips of newborn mice was routinely collected for genotyping using PCR to confirm GFP^{+} genotype.

Whole-cell current clamp recordings from morphologically identified MNs were made using an Axopatch 200B amplifier (Axon instruments), winWCP software kindly donated by Dr. J. Dempster (University of Strathclyde, Glasgow, UK) and a BNC panel block (BNC-2110, National instruments). Data were low-pass filtered (5 kHz) and digitized at 10 kHz for off-line analysis using AxographX (Axon instruments, Sydney, Australia) and Matlab (MathWorks). A hyperpolarizing or depolarizing bias current was used to maintain a resting membrane potential of −60 mV for all MNs. Only cells with a stable resting membrane potential were used for analysis. Current clamp protocols were applied independently of holding current value. Rheobase was noted as the minimum depolarizing injected current (20 pA increments, 25 ms) sufficient to evoke an action potential (AP). The first AP generated in response to the rheobase steps was further used for measuring AP properties. The AP threshold is noted as the potential when the increase in potential exceeds >50 mV/ms, AP half-width is measured at 50% of the spike amplitude

and AP delay is the time from the rheobase step onset to the AP onset (at 5% of peak amplitude).

After-hyperpolarization (AHP) amplitude, onset, rise (from 10% to 90% of peak), half-width, time to peak and half-decay time (time-point of peak to time where the membrane potential has returned halfway to the resting potential) was recorded in response to a supra-threshold current injection (3 nA, 2 ms). Input resistance was calculated from the average response to a hyperpolarizing current (−50 pA, 500 ms, 20 repetitions) that was too small in magnitude to generate any detectable hyperpolarization-activated currents (Leao et al., 2006). Hyperpolarizing and depolarizing current steps (−300 to +400 pA, 50 pA increments, 1 s duration) was used to record firing patterns of MNs. For AP firing frequency we analyzed the response to a 400 pA depolarizing current injection. The initial doublet distance notes the time (ms) between the first two APs in the train, and firing frequency was calculated as the steady state firing rate from the second half of the step (last 500 ms of the 1 s step to 400 pA). Following recordings, cells were filled with biocytin, fixed with formaldehyde (4%, 1 h) and stained with streptavidin-conjugated Alexa-594 (1:1000, Invitrogen) for 1 h. Images were collected on a Ziess LSM510 confocal microscope as stacks and collapsed into 3D image and ImageJ (NIH) was used for changing look-up tables to inverted monochrome images.

Extracellular electrophysiology

P2–P6 mice were anesthetized with isoflurane and decapitated, eviscerated and submerged in ice-cold dissection buffer oxygenated with 95% O_2/5% CO_2 containing the following (in mM: 128 NaCl, 4.69 KCl, 25 $NaHCO_3$, 1.18 KH_2PO_4, 3.5 $MgSO_4$, 0.25 $CaCl_2$ and 22 D-Glucose; equilibrated with 95% O_2 and 5% CO_2). The spinal cord was carefully dissected out of the spinal column, placed in a Sylgard-coated recording chamber and hemisected using a tungsten needle. The hemisected spinal cord was then left for >15 min to recover continuously perfused with aCSF containing the following (in mM: 128 NaCl, 4.69 KCl, 25 $NaHCO_3$, 1.18 KH_2PO_4, 1.25 $MgSO_4$, 2.5 $CaCl_2$ and 22 D-Glucose; equilibrated with 95% O_2 and 5% CO_2).

Dorsal and ventral lumbar level 2 or 3 roots were inserted into glass suction electrodes. Dorsal roots were stimulated using a stimulus isolator unit (A365, World precision instruments) with 0.2 ms current pulses of increasing intensity (0–30 μA), until maximal reflex amplitude was reached. For recording stimulus, intensity was increased to 1.5× the intensity generating maximal response (9.5–45 μA). Reflex responses were recorded in the corresponding ventral roots at alternating current (AC) with a 0.1 Hz high-pass filter and 2 kHz low-pass filter, amplified (1000 or 10 000×), and digitized at 10 kHz with a Digidata 1440A acquisition card and pClamp 10.2 software (Molecular Devices).

Traces were analyzed offline using Clampfit 10.2 (Molecular Devices). The latency was defined as the time between the stimulus artifacts until the first deflection in potential (monosynaptic) or second deflection potential (polysynaptic). The amplitude was measured as the largest peak following the monosynaptic and polysynaptic deflections. The polysynaptic area was calculated as the area under the curve from the second deflection peak and the following 80 ms between trace and baseline. The experimenter was blinded to the genotype during experiments and analysis.

Cluster analysis

A clustering algorithm was written in the R statistical computer environment (Version 2.11.1) (R Development Core Team, 2010). After standardization of the variables (Supplementary Table 1) the optimal number of clusters for GFP^- MN data was computed using 'within-groups' sum-of-squares. Standard analysis of the descriptive statistics was applied and agglomerative hierarchical clustering (Ward's method) was chosen as the most fitting method for the data set (Ward, 1963). The linkage function (value of the "distance" between two groups of objects) of the Ward's method was computed as the increase in the error sum of squares (ESS). If X stands for our data matrix of values, ESS is the sum of squares of the deviations from the mean value or the mean vector.

$$\mathrm{ESS}(X) = \sum_{i=1}^{N_x} |x_i - \frac{1}{N_x}\sum_{j=1}^{N_x} x_j|$$

Mathematically, the linkage function of our two clusters of interest is described by the following expression

$$\mathrm{D}(\mathrm{S},\mathrm{F}) = \mathrm{ESS}(\mathrm{SF}) - [\mathrm{ESS}(\mathrm{S}) + \mathrm{ESS}(\mathrm{F})]$$

where S stands for the cluster of slow alpha MNs, F for the cluster of fast alpha MNs and SF is the combined cluster resulting from fusion clusters S and F. At each step in the analysis, the union of every possible cluster pair was considered and the two clusters whose fusion results in minimum increase in 'information loss' were combined. In order to avoid the noise of variables that are highly correlated with each other, the Bayesian variables selection method was used (Albert, 2009; Koch, 2007). Principal component analysis found all 16 parameters important for the clustering result.

Quantification of histological staining

The sections used for quantification, as stated in the corresponding results section, contain information on the spinal cord region, muscle type and age of the animals. In general, soma area calculation was performed after *in situ* hybridization on 60 μm sections as previously described (Enjin et al., 2010). Sections were monitored carefully during color development to prevent excessive staining. Only cells with the whole nucleus surrounded by staining were selected for quantification. Cell perimeter was manually outlined and the soma area was calculated using the imaging program Volocity (*5-ht1d* and *VAChT* double *in situ* hybridization) or ImageJ (*5-ht1d*$^{-/-}$ and *Egr3*$^{-/-}$ mutants) software. Counting of *5-ht1d*$^{+}$ cells in *Egr3*$^{-/-}$ spinal cord was performed under microscope in the lateral motor column region after *in situ* hybridization. Muscle spindle innervation was measured as the number of *VAChT*$^{+}$/Bungarotoxin^{+} sites per 50 μm Calbindin-stained muscle spindle on a collapsed z-stack of optically scanned confocal images at 0.99 μm obtained at 20×, 0.8 numerical aperture, and 1024×1024 pixels. Sensory innervation of MNs was calculated by counting the number of VGLUT1^{+} puncta in direct connection with a ChAT^{+} motor neuron soma or proximal dendrite in a z-series of 15 optically scanned confocal images at 1.02 μm obtained at 63×, 1.4 numerical aperture, and 2048×2048 pixels. The number of counted MNs is stated in the results section.

Motor coordination test

Ten *5-ht1d*$^{+/+}$ and ten *5-ht1d*$^{-/-}$ mice were subjected to three different motor coordination tasks (Rotarod, Beam walking and Hanging wire tests). Mice were excluded from a specific test if the experiment exceeded the given maximum duration. The experimenter was blind to genotype while performing and analyzing experiments.

The Rotarod performance test was carried out on 25 weeks old mice using a commercial Rotorod (IITC life science Inc., Woodland Hills, CA). The experiment was performed as three trials per day for three consecutive days. Each trial was separated by at least 15 min. The best trial from each day was used for analysis. The rods accelerated from 0 to 45 rpm during 60 s and then kept at maximum speed for another 60 s. The rotation speed at which the mice fell from the rod was automatically recorded. When the sensor failed to detect a mouse falling off this was manually registered. If an animal was

clinging on to the rods for 1–2 rotations before falling off the rod the trail was still included in the experiment.

The beam walking balance test was performed on 3 weeks old mice. The experiment was performed on a one-meter long rounded wooden beam. Mice were allowed to learn the task with two test runs on a rod of 25 mm diameter. The experiment was conducted on a rod of 12 mm diameter. The duration for crossing the beam was noted and mice were video recorded from behind for further analysis of hind paw foot slips. Each mouse was given three trials and the maximum duration of the beam-walking test was set to 15 s to exclude animals that did not cross the beam. This excluded two *5-ht1d*$^{+/+}$ and three *5-ht1d*$^{-/-}$ mice from the analysis.

The hanging wire challenge was performed on 24 weeks old mice. Mice were held by the tail so they could grip a metal wire with the forepaws and then carefully released. The time of how long it took to climb up with one of the hind paws onto the metal wire was measured. An immediate climb upon placing the mouse on the wire was noted as <1 s, and >1 s indicates that the mouse struggled to climb up the wire. Each mouse was given three trials and the maximum test duration was set to 30 s, which excluded one *5-ht1d*$^{-/-}$ mouse from the analysis. The trial in which the animal accomplished the task in the shortest time was used for analysis.

Statistical analyses

All data are expressed as mean ± SEM values. Groups were compared using unpaired two-tailed Student's *t*-test for parametric data and Mann–Whitney *U*-test for non-parametric data. Whole-cell electrophysiology data showed normal distribution (Kolmigorov–Smirnov test) and was analyzed using one-way ANOVA or two-tailed two-sample equal variance Student *t*-test as seen fit. The Chi square test was used for nominal data. Probability levels <0.05 were considered statistically significant.

Supplementary materials related to this article can be found online at doi:10.1016/j.mcn.2012.01.003.

Acknowledgements

We thank Dr. S. Nakanishi for advice. This work was supported by grants from the Swedish Medical Research Council (KK, KL), National Institutes of Health (NIH), R01-NS040748 (WGT), K26-RR026099 (WGT), the International Institute for Research on Paraplegia, the Swedish Brain Foundation and the foundations of Åke Wiberg, Åhlén, Hedlund, Göran Gustafsson and Uppsala University. KK is a Royal Swedish Academy of Sciences Research Fellow supported by a grant from the Knut and Alice Wallenberg Foundation.

References

Albert, J., 2009. Baysian Computation with R, 2nd ed. Springer-verlag Gmbh.
Betley, J.N., Wright, C.V., Kawaguchi, Y., Erdelyi, F., Szabo, G., Jessell, T.M., Kaltschmidt, J.A., 2009. Stringent specificity in the construction of a GABAergic presynaptic inhibitory circuit. Cell 139, 161–174.
Bonnin, A., Torii, M., Wang, L., Rakic, P., Levitt, P., 2007. Serotonin modulates the response of embryonic thalamocortical axons to netrin-1. Nat. Neurosci. 10, 588–597.
Bryan, R.N., Trevino, D.L., Willis, W.D., 1972. Evidence for a common location of alpha and gamma motoneurons. Brain Res. 38, 193–196.
Burke, R.E., Fyffe, R.E., Moschovakis, A.K., 1994. Electrotonic architecture of cat gamma motoneurons. J. Neurophysiol. 72, 2302–2316.
Burke, R.E., Strick, P.L., Kanda, K., Kim, C.C., Walmsley, B., 1977. Anatomy of medial gastrocnemius and soleus motor nuclei in cat spinal cord. J. Neurophysiol. 40, 667–680.
Chen, H.H., Tourtellotte, W.G., Frank, E., 2002. Muscle spindle-derived neurotrophin 3 regulates synaptic connectivity between muscle sensory and motor neurons. J. Neurosci. 22, 3512–3519.
Cole, J.D., Sedgwick, E.M., 1992. The perceptions of force and of movement in a man without large myelinated sensory afferents below the neck. J. Physiol. 449, 503–515.
Comery, B., Marini, J.F., Gardiner, P.F., 2000. Changes in electrophysiological properties of tibial motoneurons in the rat following 4 weeks of tetrodotoxin-induced paralysis. Neurosci. Lett. 287, 21–24.
Djupsjobacka, M., Johansson, H., Bergenheim, M., Wenngren, B.I., 1995. Influences on the gamma-muscle spindle system from muscle afferents stimulated by increased intramuscular concentrations of bradykinin and 5-HT. Neurosci. Res. 22, 325–333.
Dugue, G.P., Dumoulin, A., Triller, A., Dieudonne, S., 2005. Target-dependent use of co-released inhibitory transmitters at central synapses. J. Neurosci. 25, 6490–6498.
Eccles, J.C., Eccles, R.M., Iggo, A., Lundberg, A., 1960. Electrophysiological studies on gamma motoneurones. Acta Physiol. Scand. 50, 32–40.
Edamura, M., Yang, J.F., Stein, R.B., 1991. Factors that determine the magnitude and time course of human H-reflexes in locomotion. J. Neurosci. 11, 420–427.
Emonet-Denand, F., Jami, L., Laporte, Y., 1975. Skeleto-fusimotor axons in the hindlimb muscles of the cat. J. Physiol. 249, 153–166.
Enjin, A., Rabe, N., Nakanishi, S.T., Vallstedt, A., Gezelius, H., Memic, F., Lind, M., Hjalt, T., Tourtellotte, W.G., Bruder, C., Eichele, G., Whelan, P.J., Kullander, K., 2010. Identification of novel spinal cholinergic genetic subtypes disclose Chodl and Pitx2 as markers for fast motor neurons and partition cells. J. Comp. Neurol. 518, 2284–2304.
Frank, E., Wenner, P., 1993. Environmental specification of neuronal connectivity. Neuron 10, 779–785.
Friese, A., Kaltschmidt, J.A., Ladle, D.R., Sigrist, M., Jessell, T.M., Arber, S., 2009. Gamma and alpha motor neurons distinguished by expression of transcription factor Err3. Proc. Natl. Acad. Sci. U. S. A. 106, 13588–13593.
Fujiyama, F., Furuta, T., Kaneko, T., 2001. Immunocytochemical localization of candidates for vesicular glutamate transporters in the rat cerebral cortex. J. Comp. Neurol. 435, 379–387.
Gardiner, P.F., 1993. Physiological properties of motoneurons innervating different muscle unit types in rat gastrocnemius. J. Neurophysiol. 69, 1160–1170.
Gaspar, P., Cases, O., Maroteaux, L., 2003. The developmental role of serotonin: news from mouse molecular genetics. Nat. Rev. 4, 1002–1012.
Gong, S., Zheng, C., Doughty, M.L., Losos, K., Didkovsky, N., Schambra, U.B., Nowak, N.J., Joyner, A., Leblanc, G., Hatten, M.E., Heintz, N., 2003. A gene expression atlas of the central nervous system based on bacterial artificial chromosomes. Nature 425, 917–925.
Gosgnach, S., Quevedo, J., Fedirchuk, B., McCrea, D.A., 2000. Depression of group Ia monosynaptic EPSPs in cat hindlimb motoneurones during fictive locomotion. J. Physiol. 526 (Pt 3), 639–652.
Granados-Soto, V., Arguelles, C.F., Rocha-Gonzalez, H.I., Godinez-Chaparro, B., Flores-Murrieta, F.J., Villalon, C.M., 2010. The role of peripheral 5-HT1A, 5-HT1B, 5-HT1D, 5-HT1E and 5-HT1F serotonergic receptors in the reduction of nociception in rats. Neuroscience 165, 561–568.
Haydon, P.G., McCobb, D.P., Kater, S.B., 1984. Serotonin selectively inhibits growth cone motility and synaptogenesis of specific identified neurons. Science (New York, N.Y.) 226, 561–564.
Hermanson, E., Joseph, B., Castro, D., Lindqvist, E., Aarnisalo, P., Wallen, A., Benoit, G., Hengerer, B., Olson, L., Perlmann, T., 2003. Nurr1 regulates dopamine synthesis and storage in MN9D dopamine cells. Exp. Cell Res. 288, 324–334.
Hietanen-Peltola, M., Pelto-Huikko, M., Rechardt, L., Emson, P., Hokfelt, T., 1992. Calbindin D-28k-immunoreactivity in rat muscle spindle; a light and electron microscopic study. Brain Res. 579, 327–332.
Honda, C.N., 1995. Differential distribution of calbindin-D28k and Parvalbumin in somatic and visceral sensory neurons. Neuroscience 68, 883–892.
Jovanovic, K., Anastasijevic, R., Vuco, J., 1990. Reflex effects on gamma fusimotor neurones of chemically induced discharges in small-diameter muscle afferents in decerebrate cats. Brain Res. 521, 89–94.
Kanning, K.C., Kaplan, A., Henderson, C.E., 2010. Motor neuron diversity in development and disease. Annu. Rev. Neurosci. 33, 409–440.
Kernell, D., Bakels, R., Copray, J.C., 1999. Discharge properties of motoneurones: how are they matched to the properties and use of their muscle units? J. Physiol. Paris 93, 87–96.
Koch, K.-R., 2007. Parameter estimation, confidence regions and hypothesis testing, Introduction to Bayesian statistics, 2nd ed. Springer-verlag Gmbh, New York, pp. 63–73.
Kullander, K., 2005. Genetics moving to neuronal networks. Trends Neurosci. 28, 239–247.
Lagerback, P.A., 1985. An ultrastructural study of cat lumbosacral gamma-motoneurons after retrograde labelling with horseradish peroxidase. J. Comp. Neurol. 240, 256–264.
Leao, K.E., Leao, R.N., Sun, H., Fyffe, R.E.W., Walmsley, B., 2006. Hyperpolarization-activated currents are differentially expressed in mice brainstem auditory nuclei. J. Physiol. 576.3, 849–864.
Llewellyn, M., Yang, J.F., Prochazka, A., 1990. Human H-reflexes are smaller in difficult beam walking than in normal treadmill walking. Experimental brain research. Exp. Hirnforsch. 83, 22–28.
Mentis, G.Z., Alvarez, F.J., Shneider, N.A., Siembab, V.C., O'Donovan, M.J., 2010. Mechanisms regulating the specificity and strength of muscle afferent inputs in the spinal cord. Ann. N. Y. Acad. Sci. 1198, 220–230.
Nakanishi, S.T., Whelan, P.J., 2010. Diversification of intrinsic motoneuron electrical properties during normal development and botulinum toxin-induced muscle paralysis in early postnatal mice. J. Neurophysiol. 103, 2833–2845.
Pape, H.C., 1996. Queer current and pacemaker: the hyperpolarization-activated cation current in neurons. Annu. Rev. Physiol. 58, 299–327.
Pflieger, J.F., Clarac, F., Vinay, L., 2002. Postural modifications and neuronal excitability changes induced by a short-term serotonin depletion during neonatal development in the rat. J. Neurosci. 22, 5108–5117.

R Development Core Team, 2010. R: A language and environment for statistical computing. R Foundation for Statistical Computing, Vienna, Austria.
Rossignol, S., Dubuc, R., Gossard, J.P., 2006. Dynamic sensorimotor interactions in locomotion. Physiol. Rev. 86, 89–154.
Schwartz, E.J., Gerachshenko, T., Alford, S., 2005. 5-HT prolongs ventral root bursting via presynaptic inhibition of synaptic activity during fictive locomotion in lamprey. J. Neurophysiol. 93, 980–988.
Scott, J.J., Kummel, H., Illert, M., 1995. Skeletofusimotor (beta) innervation of proximal and distal forelimb muscles of the cat. Neurosci. Lett. 190, 1–4.
Shneider, N.A., Brown, M.N., Smith, C.A., Pickel, J., Alvarez, F.J., 2009a. Gamma motor neurons express distinct genetic markers at birth and require muscle spindle-derived GDNF for postnatal survival. Neural Dev. 4, 42.
Shneider, N.A., Mentis, G.Z., Schustak, J., O'Donovan, M.J., 2009b. Functionally reduced sensorimotor connections form with normal specificity despite abnormal muscle spindle development: the role of spindle-derived neurotrophin 3. J. Neurosci. 29, 4719–4735.
Stamford, J.A., Davidson, C., McLaughlin, D.P., Hopwood, S.E., 2000. Control of dorsal raphe 5-HT function by multiple 5-HT(1) autoreceptors: parallel purposes or pointless plurality? Trends Neurosci. 23, 459–465.
Stankovski, L., Alvarez, C., Ouimet, T., Vitalis, T., El-Hachimi, K.H., Price, D., Deneris, E., Gaspar, P., Cases, O., 2007. Developmental cell death is enhanced in the cerebral cortex of mice lacking the brain vesicular monoamine transporter. J. Neurosci. 27, 1315–1324.
Strick, P.L., Burke, R.E., Kanda, K., Kim, C.C., Walmsley, B., 1976. Differences between alpha and gamma motoneurons labeled with horseradish peroxidase by retrograde transport. Brain Res. 113, 582–588.
Tourtellotte, W.G., Keller-Peck, C., Milbrandt, J., Kucera, J., 2001. The transcription factor Egr3 modulates sensory axon-myotube interactions during muscle spindle morphogenesis. Dev. Biol. 232, 388–399.
Tourtellotte, W.G., Milbrandt, J., 1998. Sensory ataxia and muscle spindle agenesis in mice lacking the transcription factor Egr3. Nat. Genet. 20, 87–91.
Wallen-Mackenzie, A., Gezelius, H., Thoby-Brisson, M., Nygard, A., Enjin, A., Fujiyama, F., Fortin, G., Kullander, K., 2006. Vesicular glutamate transporter 2 is required for central respiratory rhythm generation but not for locomotor central pattern generation. J. Neurosci. 26, 12294–12307.
Ward, J., 1963. Hierarchical grouping to optimize an objective function. J. Am. Stat. Assoc. 58, 236.
Westbury, D.R., 1982. A comparison of the structures of alpha and gamma-spinal motoneurones of the cat. J. Physiol. 325, 79–91.
Whitehead, J., Keller-Peck, C., Kucera, J., Tourtellotte, W.G., 2005. Glial cell-line derived neurotrophic factor-dependent fusimotor neuron survival during development. Mech. Dev. 122, 27–41.
Zengel, J.E., Reid, S.A., Sypert, G.W., Munson, J.B., 1985. Membrane electrical properties and prediction of motor-unit type of medial gastrocnemius motoneurons in the cat. J. Neurophysiol. 53, 1323–1344.